

Number-resolved imaging of ^{88}Sr atoms in a long working distance optical tweezer

N. C. Jackson¹, R. K. Hanley^{1,2}, M. Hill¹, C. S. Adams¹, M. P. A. Jones^{1*}

¹ Joint Quantum Centre (Durham-Newcastle), Department of Physics, Durham University, DH1 3LE, United Kingdom

² Department of Physics, University of Oxford, Clarendon Laboratory, Parks Road, Oxford, OX1 3PU, United Kingdom

* m.p.a.jones@durham.ac.uk

May 19, 2022

Abstract

We demonstrate the number-resolved detection of individual strontium atoms in an optical tweezer. Using a long-working distance low numerical aperture ($\text{NA} = 0.26$) tweezer, we avoid parity projection due to light-assisted collisions, and are able to resolve up to $N = 3$ atoms within an imaging time of less than $300\text{ }\mu\text{s}$. We also discuss the methods for the measurement of the atomic temperature and trap parameters.

1 Introduction

Methods for isolating and reading out individual quantum systems are at the heart of current developments in quantum science and technology. Individually trapped neutral atoms were first observed in a magneto-optical trap (MOT) [1], and then in optical tweezers [2,3] and optical lattices [4]. Since then, the optical tweezer approach has been developed to produce addressable arrays of arbitrary geometry [5] and dimensionality [6–9] containing $N \approx 100$ atoms. Applications include quantum simulation [10,11] and computation [12], as well as quantum chemistry [13,14].

A key recent development was the extension of tweezer array techniques from alkali-metal atoms to the divalent atomic species Sr [15,16] and Yb [17]. These species have important applications in optical frequency standards [18] due to their extremely narrow ($< 1\text{ Hz}$) optical clock transitions. In combination with tweezer array technology, this highly coherent environment offers new perspectives in quantum-enhanced metrology and quantum simulation. Furthermore, narrow intercombination cooling transitions provide powerful new methods for loading [15,16] and high-fidelity imaging in tweezer arrays [19], as well as cooling to the motional ground state [16,20]. In all tweezer array experiments so far, the tightly-focused tweezers were created with high-numerical aperture ($\text{NA} > 0.5$) lenses with working distances of $< 15\text{ mm}$. This inevitably leads to the presence of dielectric surfaces close to the trapped atoms, with the potential for unwanted systematic shifts of the ultra-narrow clock transitions [21,22].

In this paper we present the isolation and detection of individual strontium atoms in an optical tweezer with a working distance of 37 mm ($\text{NA} = 0.26$). Combined with a conductive coating on the lenses and in-vacuo electrodes, this system is designed to provide a tweezer

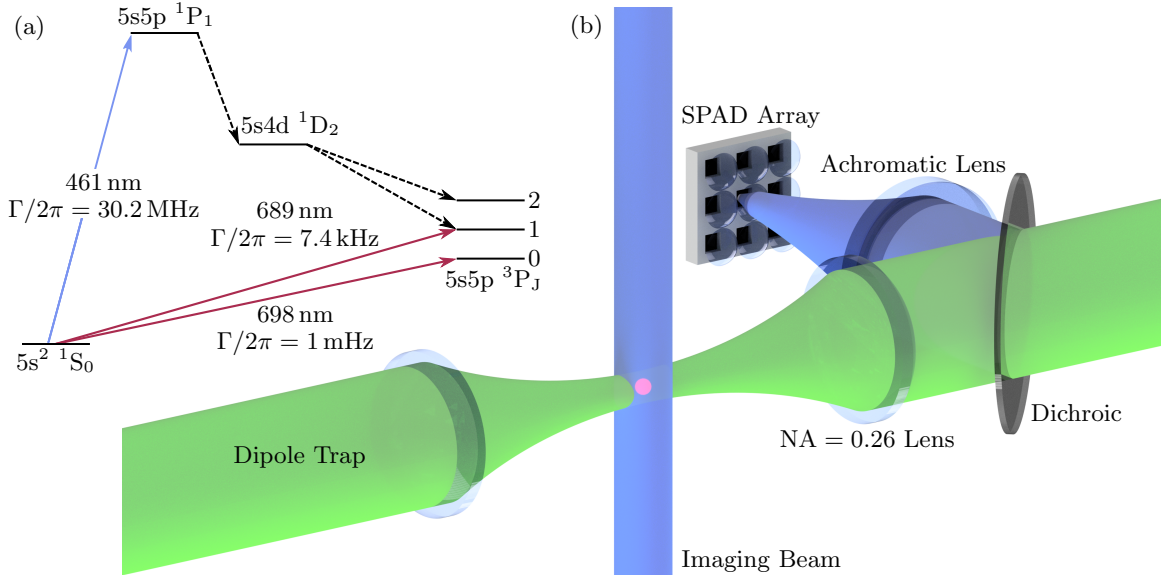


Figure 1: (a) Sr energy level diagram. (b) Experimental set-up. Strontium atom(s) are trapped in a 532 nm optical tweezer formed by the NA = 0.26 aspheric lenses. A 461 nm probe beam is used to image the atom(s), with the resulting fluorescence collected through one of the aspheric lenses and imaged onto the SPAD camera via its integrated microlens array.

array platform compatible with precision measurement, and in particular with our proposal to create non-classical states in optical atomic clocks using Rydberg states [23]. We observe that it is possible to load ultra-cold atoms into the tweezer directly from a magneto-optical trap operating on a narrow intercombination line, even when the differential AC Stark shift on the cooling transition is significant, in agreement with the results in [19]. By subsequently ramping adiabatically to much deeper traps, we show that the trapped atoms can be imaged without loss due to light-assisted collisions, avoiding the projection of the atom number in the trap onto either zero or one commonly observed in tweezer experiments. As a result we can distinguish states of $N = 0 - 3$ atoms in the tweezer within in 300 μ s. Monitoring the decay of the trapped atom number could provide a route to quasi-deterministic preparation of single-atom states without transport, and with an overall efficiency that is comparable to the current state-of-the-art of 90% obtained using light-assisted collisions [24–26].

2 Long-working distance optical tweezer

A schematic of the experiment is shown in Fig. 1, and a detailed description is provided in [27]. The optical tweezer is created by focusing a 532 nm trapping beam to a waist of 1.28(1) μ m using a custom aspheric lens with a numerical aperture of 0.26, mounted inside an ultra-high vacuum (UHV) chamber. The lens has a broadband anti-reflection coating on the input side, and a transparent conductive indium tin oxide (ITO) coating on the side facing the atoms. Such ITO coatings have proven essential in reducing stray electric fields in previous experiments with Rydberg atoms in optical tweezers. The lens design was optimised

for trapping at 532 nm and at the 813 nm magic wavelength for the clock transition, as well as for collection of the fluorescence at 461 nm.

Compared to similar optical tweezer setups based on in-vacuo lenses [15], the working distance in our experiment (37 mm) is a factor of > 2 larger. The difference is even more significant compared to experiments based on air-side objectives and glass cells [16], where the atom-surface distance may be only a few millimetres. This feature of our apparatus is important since the presence of nearby surfaces has been shown to lead to significant shifts in Rydberg energy levels [28, 29] and in optical atomic clock experiments [21]. Even for conductive surfaces, the presence of adsorbates may lead to significant unwanted fields [30]. Here we trade off this potential for a low-field environment against the numerical aperture of the objective. However as we show in section 6, we are still able to detect single atoms.

On the opposite side of the UHV chamber, an identical objective collects and recollimates the trapping light. Between the lenses, two planar arrays of 6 electrodes enable electric fields to be applied along all the available optical axes. A pair of coils mounted inside the vacuum provide a strong quadrupole field for the MOT, as well as the ability to apply static fields of up to 8 mT. The latter will enable us to exploit the clock transition in the bosonic isotopes of strontium [31–33].

3 Avalanche Photodiode Array Detector

Conventionally, tweezer array experiments rely on either single-pixel Single Photon Avalanche Diode detectors (SPADs), or on intensified or electron-multiplying CCD cameras as detectors. Recently sCMOS cameras have also been investigated [34]. Single-pixel SPADs have the advantage of true photon counting and nanosecond time resolution, making them useful for experiments in quantum optics, but are difficult to scale to large numbers of traps. Conversely, CCD or sCMOS cameras have higher noise and relatively slow frame rates, but enable the simultaneous readout of arrays containing thousands of trap if required.

In this paper we follow a different approach, based on a commercially available SPAD array detector (Micro Photon Devices SPC3). The array consists of 64×32 pixels, each of which is an independent SPAD [35]. Independent counters are provided for each pixel that return the number of detected photons within the gated exposure time, which may be as short as 1.5 ns. Full-frame readout of the camera is possible at 9.6×10^4 frames per second. The measured dark count distribution is shown in Fig. 2(a), with $> 95\%$ of the pixels having a dark count below 100 s^{-1} . The measured quantum efficiency at 461 nm is 36(2)%. Compared to CCD or sCMOS technology (see [34] for a useful comparison), the SPAD array detector provides better signal-to-noise ratio at extremely low light level, while maintaining a high readout speed. The sensitivity and low noise of this detector is an important factor in our ability to detect single atoms with our reduced NA. As we show in section 6, the fast readout enables real-time monitoring of the trap occupancy with sub-millisecond resolution for deterministic loading protocols.

An important difference between the SPAD array and an EMCCD camera is the pixel size. The SPAD pixels are large ($150 \mu\text{m} \times 150 \mu\text{m}$), with an active area of $30 \mu\text{m} \times 30 \mu\text{m}$ at the centre. An integrated microlens in front of each pixel boosts the collection efficiency to 85% of the chip surface. Nevertheless, the large pixel size means a substantial overall magnification is required. For the experiments presented here with a single tweezer, we use

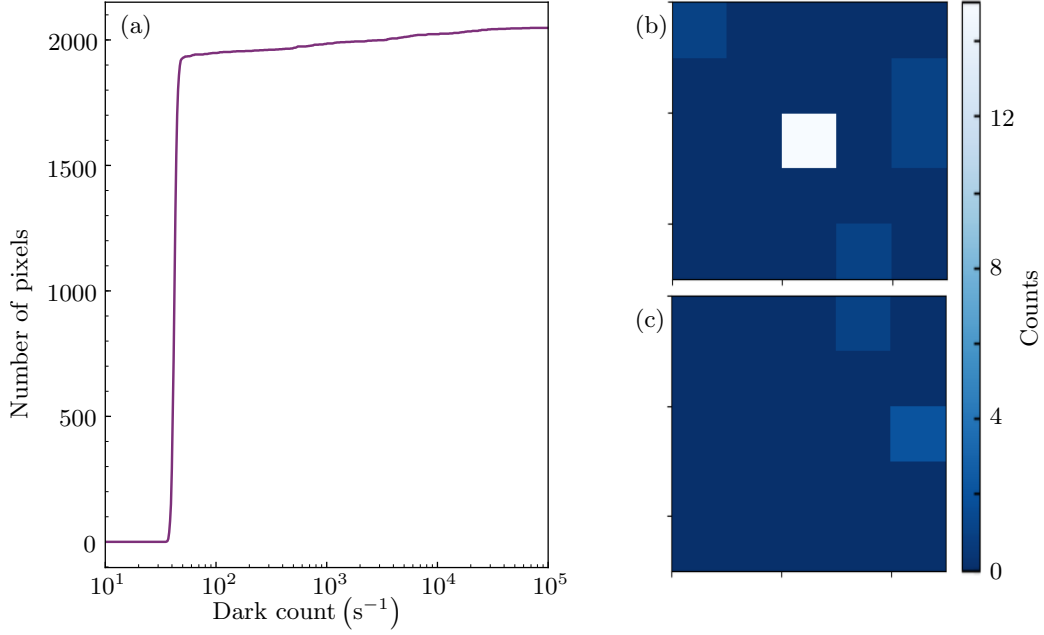


Figure 2: (a) Measured cumulative distribution function of the dark count over the SPAD array. (b) and (c) Images obtained on the sensor after 1 ms of exposure time, over an area of 5×5 pixels, in the presence (b) and absence (c) of a single atom.

an overall magnification of ten, giving an effective pixel size in the object plane of $15 \mu\text{m}$. Thus all the light from the dipole trap is concentrated on a single pixel. For future experiments with trap arrays, the magnification will be boosted by an additional telescope. In tandem with control over the array spacing using spatial light modulators, the SPAD array should provide a flexible readout device for arrays of > 1000 traps.

4 Loading the tweezer

The optical tweezer is loaded from a narrow-line magneto optical trap (nMOT) operating on the $5s^2^1S_0 \rightarrow 5s5p^3P_1$ line at 689 nm. The nMOT itself is loaded using the conventional sequence of pre-cooling on the broad $5s^2^1S_0 \rightarrow 5s5p^1P_1$ transition at 461 nm, followed by transfer to a “broadband” cooling phase of duration 150 ms on the 689 nm transition. The tweezer beam is turned on throughout the nMOT phase, which lasts for 100 ms. To control the density of the nMOT, and hence the number of atoms loaded into the tweezer, we vary the duration of the pre-cooling step from 10 to 100 ms. After a variable hold time, atoms in the tweezer are imaged using a pulse of light on the $5s^2^1S_0 \rightarrow 5s5p^1P_1$ transition, with the resulting fluorescence collected and imaged onto the SPAD array as shown in Fig. 2. For the data in this section and the next, where the trap was loaded with many atoms, the blue cooling beams were used as the imaging light. To get down to single atom sensitivity, we added an additional probe beam as shown in Fig. 1 which propagated orthogonal to the trap beam. Empirically we find that this alignment with the axis of tightest confinement is essential to avoid atoms being pushed along the trap axis during imaging.

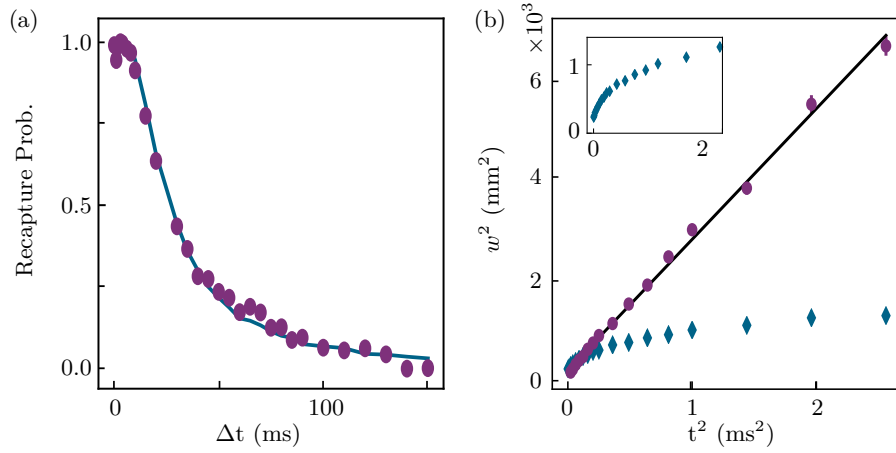


Figure 3: (a) Release and recapture measurement in a ramped trap (purple circles) with fit to the data (blue line). (b) Ballistic expansion measurement in a ramped trap (purple circles) and without ramping (blue diamonds) for same parameters as in (a), where the temperature obtained from the fit (black line) agrees with that obtained in (a).

To our surprise, we found that very deep tweezers could be loaded directly from the nMOT, despite the differential AC Stark shift on the cooling transition far exceeding its linewidth, and despite the relatively small number of photons that can be scattered during the time it takes a 1 μK atom in the nMOT to cross the tweezer. We attribute this efficient loading to the presence of a substantial fraction of atoms in the tail of the Boltzmann distribution that are moving slowly enough to scatter many photons [27]. The attractive Sisyphus type cooling mechanisms described in [19] also play a role. We find that for trap depths $U_0/k_B > 30 \mu\text{K}$, atoms can also be loaded into subsidiary intensity maxima formed by diffraction of the trapping beam by the circular aperture of the aspheric lenses. These additional traps are directly visible as an increase in the size of the imaged atom cloud, and their presence was also apparent in the temperature measurements described below. To avoid these effects, we first loaded atoms into a tweezer of depth $U_0/k_B = 10 \mu\text{K}$, before ramping to the final tweezer depth U_F over a time 1 s.

To measure the temperature of the trapped atoms, we extended two methods previously developed for alkali-metal atoms. The first is the conventional ballistic expansion technique. In order to achieve sufficient signal-to-noise, these experiments are carried out with a large number of trapped atoms, though the method has been applied to single atoms [36]. The second method is a release and recapture technique described in [37]. Here, the trap is turned back on at some point during the expansion to recapture the atoms. A temperature is extracted from the measured decay of the recaptured atom number as a function of expansion time using comparison with a Monte-Carlo simulation.

A typical release and recapture signal is shown in Fig. 3(a), along with the best fit from the Monte-Carlo simulation which yields a temperature of $24.0(1.0) \mu\text{K}$. This result is in excellent agreement with that obtained from the ballistic expansion method ($24.8(4) \mu\text{K}$) for the same trap. We note that this agreement is only found if the trap depth is ramped. For the case where atoms are loaded directly into deep traps, both methods yield unreliable results due to the presence of colder atoms trapped in subsidiary maxima, as illustrated for the ballistic

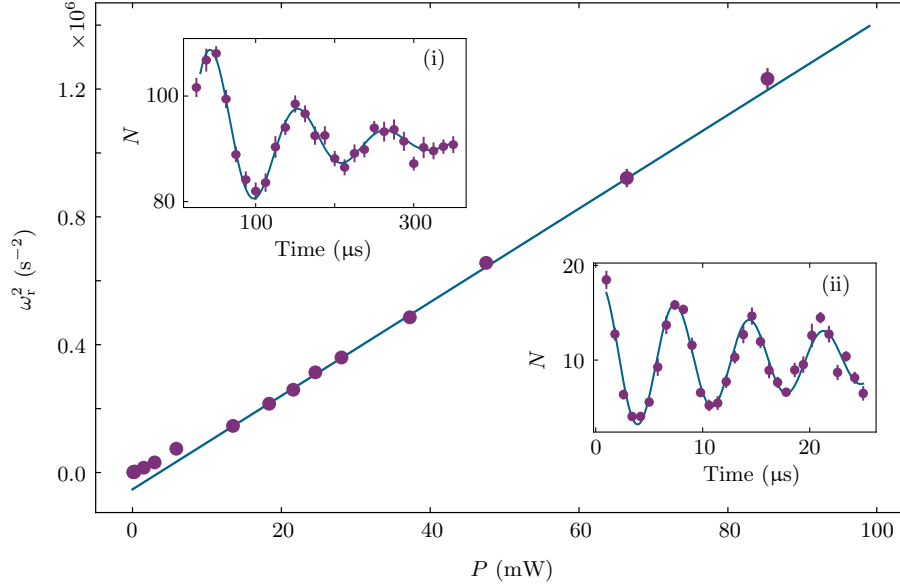


Figure 4: The square of the radial trap frequency ω_r^2 as a function of the trap power P . The fit to the data is a straight line (dark blue) which excludes the data at low trap powers. Insets show the trap frequency measurements taken at two different powers of (i) 0.3 mW and (ii) 20 mW after ramping.

expansion method in Fig. 3(b).

Lastly, we note that due to the very efficient cooling that occurs during loading, and the adiabatic nature of the ramp, we are able to prepare very cold atoms in deep traps. We find that we can achieve a ratio $U_F/(k_B T) \approx 50$ for traps up to 5 mK deep.

5 Characterizing the tweezer

For cold atoms trapped in the harmonic part of the tweezer potential, the key parameters describing the trapping are the trap depth U_F and the radial and axial trap frequencies ω_r and ω_z . Independent measurements of these quantities yield information on the trapping beam such as the waist size.

In recent work with Sr atoms, trap frequencies were empirically obtained by observing motional sidebands on the $5s^2\ ^1S_0 \rightarrow 5s5p\ ^3P_1$ transition [16]. However this technique only works well in a magic-wavelength trap, where the upper and lower states have the same polarizability (and hence the same harmonic energy level spacing). In larger dipole traps parametric heating is often used [38], but we find in common with others that this method does not work so well for deep tweezer potentials with high axial confinement. Instead we generalize a release-and-recapture technique developed for alkali-metal atoms [39].

The technique involves turning the trap off for two short periods of fixed duration t_1 and t_2 , separated by a variable duration Δt where the trap is on. The first dark period t_1 imparts a well-defined phase to the oscillations in the trap; the subsequent probability of losing the atoms during t_2 depends on whether the atoms are at a turning point of their motion and

hence on the trap frequency.

Examples of the resulting oscillations in the recapture probability are shown in the insets in Fig. 4. Since the atoms are significantly colder than in previous work with Rb, the optimal release times were found to be longer with $t_1 = 5\mu\text{s}$ ($25\mu\text{s}$) and $t_2 = 20\mu\text{s}$ ($60\mu\text{s}$) for deep (shallow) trap depths. The data in Fig. 4 are well described by a damped sine wave, from which we obtain a measurement of the radial trap frequency after correcting for the damping.

Fig. 4 shows ω_r^2 as a function of the trap power P over a large range of trap depths. From the gradient it is possible to extract the trap waist w_0 . In the harmonic approximation, the trap frequency as a function of power is given by $\omega_r^2 = 4\alpha_0 P / (m\pi\epsilon_0 c w_0^4)$ where α_0 is the ground state polarizability. The value of α_0 is dominated by the strong $5s^2\ ^1S_0 \rightarrow 5s5p\ ^1P_1$ transition, and can be calculated to high accuracy. From the gradient of the fit in Fig. 4 we find $w_0 = 1.28(1)\ \mu\text{m}$. We exclude points at lower trap powers, as otherwise we obtain a poor fit to the data. We attribute the poor fit at lower trap powers to the small ratio of the atomic temperature to trap depth, rendering the harmonic approximation invalid. This is further highlighted by the insets, where significantly higher damping is seen at lower trap powers.

6 Number-resolved imaging

Previous work with tweezer arrays of Sr has focused on using narrow-line laser cooling to enable imaging in shallow traps. Here we take a different approach, and image the atoms directly in a deep trap without cooling. The probe beam shown in Fig. 1 is tuned to the AC Stark shifted resonance of the trapped atom(s) to maximise the scattering rate. The frequency shift is determined spectroscopically as a function of trap depth, with a measured shift of 26(1) (56(1)) MHz/mK for the $|m_j| = 1$ ($|m_j| = 0$) states. For the trap depths used here, the splitting between the magnetic sublevels is resolved. The vertically propagating imaging beam is linearly polarised in the horizontal direction, for maximal coupling to the $|m_j| = 1$ state. The saturation parameter of the imaging beam, $S = I/I_{\text{sat}}$ is ~ 0.14 .

To image single atoms, we load into a $U_F/k_B = 7.5\ \text{mK}$ tweezer. The atom number is reduced to a single atom in the trap by reducing the duration of the pre-cooling stage to typically 18 ms. In Fig. 5(a) either zero or one atoms is loaded. The histogram shows the detected photons over a 1 ms imaging time, for ~ 1000 experimental repeats. The two peaks correspond to the background level of 0.1 cts/ms and to the single atom fluorescence level of 15 cts/ms. In Fig. 5(b) the loading time of the blue MOT is increased by 2 ms. The histogram shows additional peaks which correspond to two and three atoms in the trap. The additional peaks imply that we image without loss due to light-assisted collisions, avoiding the projection of the atom number in the trap onto either zero or one. We believe that light-assisted collisions reported in other experiments with Sr [15, 16] are avoided here due to the larger trap volume and higher temperature in our experiment.

The fit to the histograms in Fig. 5 is based on a Poisson distribution for both the trapped atom number and the number of photons detected per atom in each experimental run. The resulting computer-generated distributions are corrected for one-body loss due to the weak decay channel $5s5p\ ^1P_1 \rightarrow 5s4d\ ^1D_2$ [40]. At 532 nm the 1D_2 state is strongly anti-trapped, therefore any decay into this state leads to loss. To include this decay, a weighted average of histograms with different mean atom number is performed, with the weighting reflecting the exponential decay of the atom number during the imaging time. The free parameters are

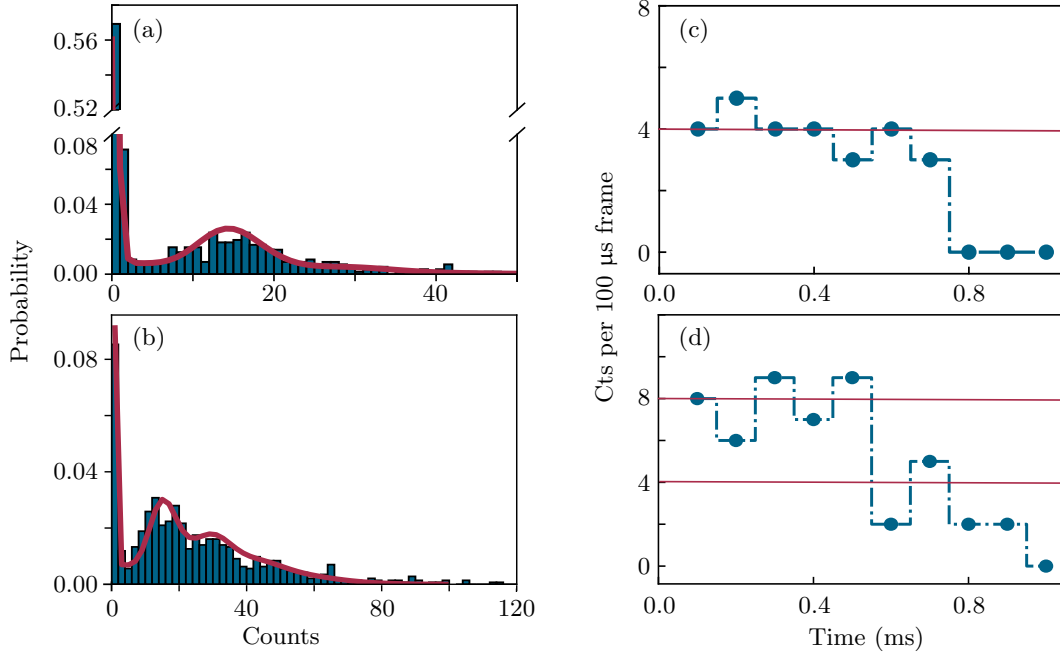


Figure 5: (a) and (b) show histograms of the number of counts after a 1 ms frame time for (a) $\bar{N} = 0.45$ (bin width of 1 count) and (b) $\bar{N} = 1.8$ (bin width of 2 counts). The red solid line is the composite Poisson distribution fit including decay described in the main text. Note that a bin width of 2 counts is used. (c) and (d) show a single atom and two atom trajectory respectively, where each point is a single 100 μ s frame. The red solid line shows the expected mean counts on the SPAD for a single atom ((d) single and two atoms).

the initial mean atom number \bar{N} , the mean number of detected photons per atom, and the effective decay rate $\bar{\Gamma}_D$ into the D state. Here a fitted decay constant of $\bar{\Gamma}_D = 3$ ms was used for both plots. We note that is smaller than the measured branching ratio for decay to the D state would suggest for resonant scattering [15,16]. We attribute this discrepancy to heating during imaging, which shifts the atoms out of resonance with the probe beam, reducing the scattering rate and hence the loss rate.

The one-body loss can also be observed in real time, as shown in Fig. 5(c) and (d), which show the time-resolved fluorescence for an individual run of the experiment. Here the 1 ms imaging time is split into ten 100 μ s frames. In Fig. 5(c) the atom is lost after 0.6 ms of imaging time, where the detected signal drops to the background level. However for the trajectory shown in (d), we observe first loss of one, and then the other atom.

Monitoring the atom number in real time as in Fig. 5(d) could provide a way to deterministically load a single atom, without the need for additional lasers or atomic transport. Initially, a few atoms would be loaded into each tweezer. Once the signal from each site is observed to drop into the range corresponding to a single atom, then the imaging light at that site would be extinguished. This could be achieved using a modification of the addressing approaches described in eg [7,41,42].

To maximise the fidelity, the probability $P(0)$ of loading no atoms must be minimised. For $\bar{N} = 1.8$ as in Fig. 5, $P(0) = 0.17$. This method would therefore already improve on the state-of-the-art demonstrated for Sr of $P(0) = 0.5$ [16,19]. Reaching the current state-of-the-

art for alkali-metal atoms (without transport) of $P(0) = 0.1$ would require $\bar{N} = 2.3$, whereas for $\bar{N} = 4$ the probability of an empty site would be just 0.01. The fidelity may also be limited by the probability of losing more than one atom during a single imaging frame. For the data in Fig. 5, the probability of losing the atom within each 100 μs frame is 0.03; the probability of losing both atoms therefore does not appear to be a significant limitation.

Experimentally, working with higher atom numbers requires further optimisation of the mean number of detected photons per atom. Currently we are not limited by our overall collection efficiency of $\eta = 0.48\%$, but by heating, which leads to a reduction in the fluorescence signal for longer exposures. This is evident in the Fig. 5, where 4 counts/atom are obtained for a 100 μs exposure but only 15 counts/atom for a 1 ms exposure. In the future this could be overcome by incorporating the Sisyphus cooling techniques developed in [19]. Further improvements could be obtained by also collecting light using the second objective. Repumping directly from the D state, or working at a trap wavelength where the D state is trapped (such as 813 nm [19]) may also provide a way to optimise the balance between one-body loss and detected signal.

7 Conclusion and Outlook

In conclusion, we have demonstrated that it is possible to trap and detect individual strontium atoms in an optical tweezer with a working distance of 37 mm. In addition, we have generalised techniques for measuring the temperature and trap parameters developed for alkali-metal atoms. Surprisingly, we find that loading from a MOT working on a narrow intercombination line is very effective, enabling cold samples of atoms to be prepared in very deep traps.

We have also shown that by using a new type of detector based on a SPAD array, it is possible individually resolve up to 3 atoms in our tweezer, and to monitor the change in atom number due to one-body loss in real time. In future experiments we plan to explore whether imaging without parity projection can be combined with cooling techniques developed elsewhere [15, 19]. By adding a spatial light modulator, we will explore whether it can be used to fill reconfigurable trap arrays with high efficiency. By combining these methods with techniques such as Rydberg dressing [43, 44], such a tweezer array could form an ideal platform for testing proposals to create highly entangled states of strontium atoms [23, 45].

Acknowledgements

We thank M. Endres and A. Browaeys for technical information. We also acknowledge the contribution of Dr P. Huillery to the early stages of the project.

Author contributions N. C. Jackson and R. K. Hanley contributed equally to this work.

Funding information This work was supported by EPSRC Responsive Mode grants EP/R035482/1 and EP/J007021/1. NCJ was supported by EPSRC Platfrom grant EP/R002061/1. The project also received funding from the European Union’s Horizon 2020 research and innovation programme under the FET grant agreement 640378-RYSQ and the EMPIR grant agreement 17FUN03-USOQS.

References

- [1] Z. Hu and H. J. Kimble, *Observation of a single atom in a magneto-optical trap*, Opt. Lett. **19**(22), 1888 (1994), doi:10.1364/OL.19.001888.
- [2] D. Frese, B. Ueberholz, S. Kuhr, W. Alt, D. Schrader, V. Gomer and D. Meschede, *Single atoms in an optical dipole trap: Towards a deterministic source of cold atoms*, Phys. Rev. Lett. **85**, 3777 (2000), doi:10.1103/PhysRevLett.85.3777.
- [3] N. Schlosser, G. Reymond, I. Protsenko and P. Grangier, *Sub-poissonian loading of single atoms in a microscopic dipole trap.*, Nature **411**, 1024 (2001), doi:https://doi.org/10.1038/35082512.
- [4] S. Kuhr, W. Alt, D. Schrader, M. Müller, V. Gomer and D. Meschede, *Deterministic delivery of a single atom*, Science **293**(5528), 278 (2001), doi:10.1126/science.1062725, <http://science.sciencemag.org/content/293/5528/278.full.pdf>.
- [5] S. Bergamini, B. Darquié, M. Jones, L. Jacubowicz, A. Browaeys and P. Grangier, *Holographic generation of microtrap arrays for single atoms by use of a programmable phase modulator*, J. Opt. Soc. Am. B **21**(11), 1889 (2004), doi:10.1364/JOSAB.21.001889.
- [6] W. Lee, H. Kim and J. Ahn, *Three-dimensional rearrangement of single atoms using actively controlled optical microtraps*, Opt. Express **24**(9), 9816 (2016), doi:10.1364/OE.24.009816.
- [7] D. Barredo, V. Lienhard, S. De Léséleuc, T. Lahaye and A. Browaeys, *Synthetic three-dimensional atomic structures assembled atom by atom*, Nature **561**(7721), 79 (2018), doi:10.1038/s41586-018-0450-2.
- [8] A. Kumar, T. Wu, F. Giraldo and D. Weiss, *Sorting ultracold atoms in a three-dimensional optical lattice in a realization of maxwell's demon*, Nature **561**(7721), 83 (2018), doi:10.1038/s41586-018-0458-7.
- [9] M. Schlosser, S. Tichelmann, M. Hambach, D. Ohl de Mello, D. Schäffner and G. Birkel, *Large-scale multilayer architecture of single-atom arrays with individual addressability*, arXiv e-prints arXiv:1902.05424 (2019), 1902.05424.
- [10] H. Bernien, S. Schwartz, A. Keesling, H. Levine, A. Omran, H. Pichler, S. Choi, A. S. Zibrov, M. Endres, M. Greiner, V. Vuletić and M. D. Lukin, *Probing many-body dynamics on a 51-atom quantum simulator*, Nature **551**, 579 (2017), doi:10.1038/nature24622.
- [11] V. Lienhard, S. de Léséleuc, D. Barredo, T. Lahaye, A. Browaeys, M. Schuler, L.-P. Henry and A. M. Läuchli, *Observing the space- and time-dependent growth of correlations in dynamically tuned synthetic ising models with antiferromagnetic interactions*, Phys. Rev. X **8**, 021070 (2018), doi:10.1103/PhysRevX.8.021070.
- [12] T. Xia, M. Lichtman, K. Maller, A. W. Carr, M. J. Piotrowicz, L. Isenhower and M. Saffman, *Randomized benchmarking of single-qubit gates in a 2d array of neutral-atom qubits*, Phys. Rev. Lett. **114**, 100503 (2015), doi:10.1103/PhysRevLett.114.100503.

- [13] L. R. Liu, J. D. Hood, Y. Yu, J. T. Zhang, N. R. Hutzler, T. Rosenband and K.-K. Ni, *Building one molecule from a reservoir of two atoms*, Science **360**(6391), 900 (2018), doi:10.1126/science.aar7797, <http://science.sciencemag.org/content/360/6391/900.full.pdf>.
- [14] L. Anderegg, L. W. Cheuk, Y. Bao, S. Burchesky, W. Ketterle, K.-K. Ni and J. M. Doyle, *An Optical Tweezer Array of Ultracold Molecules*, arXiv e-prints arXiv:1902.00497 (2019), 1902.00497.
- [15] A. Cooper, J. P. Covey, I. S. Madjarov, S. G. Porsev, M. S. Safronova and M. Endres, *Alkaline-earth atoms in optical tweezers*, Phys. Rev. X **8**, 041055 (2018), doi:10.1103/PhysRevX.8.041055.
- [16] M. A. Norcia, A. W. Young and A. M. Kaufman, *Microscopic control and detection of ultracold strontium in optical-tweezer arrays*, Phys. Rev. X **8**, 041054 (2018), doi:10.1103/PhysRevX.8.041054.
- [17] S. Saskin, J. Wilson, B. Grinkemeyer and J. Thompson, *Narrow-line cooling and imaging of Ytterbium atoms in an optical tweezer array*, arXiv e-prints arXiv:1810.10517 (2018), 1810.10517.
- [18] A. D. Ludlow, M. M. Boyd, J. Ye, E. Peik and P. O. Schmidt, *Optical atomic clocks*, Rev. Mod. Phys. **87**, 637 (2015), doi:10.1103/RevModPhys.87.637.
- [19] J. P. Covey, I. S. Madjarov, A. Cooper and M. Endres, *2000-times repeated imaging of strontium atoms in clock-magic tweezer arrays*, arXiv e-prints arXiv:1811.06014 (2018), 1811.06014.
- [20] T. Ido and H. Katori, *Recoil-free spectroscopy of neutral sr atoms in the lamb-dicke regime*, Phys. Rev. Lett. **91**, 053001 (2003), doi:10.1103/PhysRevLett.91.053001.
- [21] J. Lodewyck, M. Zawada, L. Lorini, M. Gurov and P. Lemonde, *Observation and cancellation of a perturbing dc stark shift in strontium optical lattice clocks*, IEEE Transactions on Ultrasonics, Ferroelectrics, and Frequency Control **59**(3), 411 (2012), doi:10.1109/TUFFC.2012.2209.
- [22] W. Bowden, R. Hobson, P. Huillery, P. Gill, M. P. A. Jones and I. R. Hill, *Rydberg electrometry for optical lattice clocks*, Phys. Rev. A **96**, 023419 (2017), doi:10.1103/PhysRevA.96.023419.
- [23] L. I. R. Gil, R. Mukherjee, E. M. Bridge, M. P. A. Jones and T. Pohl, *Spin squeezing in a rydberg lattice clock*, Phys. Rev. Lett. **112**, 103601 (2014), doi:10.1103/PhysRevLett.112.103601.
- [24] T. Grönzweig, A. Hilliard, M. McGovern and M. F. Andersen, *Near-deterministic preparation of a single atom in an optical microtrap*, Nature Physics **6**, 951 (2010), doi:10.1038/nphys1778.
- [25] B. J. Lester, N. Luick, A. M. Kaufman, C. M. Reynolds and C. A. Regal, *Rapid production of uniformly filled arrays of neutral atoms*, Phys. Rev. Lett. **115**, 073003 (2015), doi:10.1103/PhysRevLett.115.073003.

- [26] A. V. Carpentier, Y. H. Fung, P. Sompet, A. J. Hilliard, T. G. Walker and M. F. Andersen, *Preparation of a single atom in an optical microtrap*, Laser Physics Letters **10**(12), 125501 (2013).
- [27] R. Hanley, *Creation of a strontium microtrap: Towards a spin-squeezed atomic clock*, Ph.D. thesis, Durham University (2018).
- [28] R. P. Abel, C. Carr, U. Krohn and C. S. Adams, *Electrometry near a dielectric surface using rydberg electromagnetically induced transparency*, Phys. Rev. A **84**, 023408 (2011), doi:10.1103/PhysRevA.84.023408.
- [29] D. Neufeld, Y. Pu and F. Dunning, *Probing stray surface electric patch fields using rydberg atoms*, Nuclear Instruments and Methods in Physics Research Section B: Beam Interactions with Materials and Atoms **269**(11), 1288 (2011), doi:https://doi.org/10.1016/j.nimb.2010.11.036, INELASTIC ION-SURFACE COLLISIONS.
- [30] J. M. Obrecht, R. J. Wild and E. A. Cornell, *Measuring electric fields from surface contaminants with neutral atoms*, Phys. Rev. A **75**, 062903 (2007), doi:10.1103/PhysRevA.75.062903.
- [31] A. V. Taichenachev, V. I. Yudin, C. W. Oates, C. W. Hoyt, Z. W. Barber and L. Hollberg, *Magnetic field-induced spectroscopy of forbidden optical transitions with application to lattice-based optical atomic clocks*, Phys. Rev. Lett. **96**, 083001 (2006), doi:10.1103/PhysRevLett.96.083001.
- [32] T. Akatsuka, M. Takamoto and H. Katori, *Optical lattice clocks with non-interacting bosons and fermions*, Nature Physics **4**(12), 954 (2008).
- [33] C. Lisdat, J. S. R. V. Winfred, T. Middelmann, F. Riehle and U. Sterr, *Collisional losses, decoherence, and frequency shifts in optical lattice clocks with bosons*, Phys. Rev. Lett. **103**, 090801 (2009), doi:10.1103/PhysRevLett.103.090801.
- [34] C. J. Picken, R. Legaie and J. D. Pritchard, *Single atom imaging with an scmos camera*, Applied Physics Letters **111**(16), 164102 (2017), doi:10.1063/1.5003304, <https://doi.org/10.1063/1.5003304>.
- [35] D. Bronzi, F. Villa, S. Tisa, A. Tosi, F. Zappa, D. Durini, S. Weyers and W. Brockherde, *100 000 frames/s 64×32 single-photon detector array for 2-d imaging and 3-d ranging*, IEEE Journal of Selected Topics in Quantum Electronics **20**(6), 354 (2014), doi:10.1109/JSTQE.2014.2341562.
- [36] A. Fuhrmanek, A. M. Lance, C. Tuchendler, P. Grangier, Y. R. P. Sortais and A. Browaeys, *Imaging a single atom in a time-of-flight experiment*, New Journal of Physics **12**(5), 053028 (2010), doi:10.1088/1367-2630/12/5/053028.
- [37] C. Tuchendler, A. M. Lance, A. Browaeys, Y. R. P. Sortais and P. Grangier, *Energy distribution and cooling of a single atom in an optical tweezer*, Phys. Rev. A **78**, 033425 (2008), doi:10.1103/PhysRevA.78.033425.
- [38] S. Friebe, C. D'Andrea, J. Walz, M. Weitz and T. W. Hänsch, *co₂-laser optical lattice with cold rubidium atoms*, Phys. Rev. A **57**, R20 (1998), doi:10.1103/PhysRevA.57.R20.

- [39] H. Engler, T. Weber, M. Mudrich, R. Grimm and M. Weidemüller, *Very long storage times and evaporative cooling of cesium atoms in a quasielectrostatic dipole trap*, Phys. Rev. A **62**, 031402 (2000), doi:10.1103/PhysRevA.62.031402.
- [40] X. Xu, T. H. Loftus, J. L. Hall, A. Gallagher and J. Ye, *Cooling and trapping of atomic strontium*, J. Opt. Soc. Am. B **20**(5), 968 (2003), doi:10.1364/JOSAB.20.000968.
- [41] H. Kim, W. Lee, H.-g. Lee, H. Jo, Y. Song and J. Ahn, *In situ single-atom array synthesis using dynamic holographic optical tweezers*, Nature communications **7**, 13317 (2016), doi:10.1038/ncomms13317.
- [42] D. Stuart and A. Kuhn, *Single-atom trapping and transport in DMD-controlled optical tweezers*, New Journal of Physics **20**(2), 023013 (2018), doi:10.1088/1367-2630/aaa634.
- [43] J. Zeiher, P. Schauß, S. Hild, T. Macrì, I. Bloch and C. Gross, *Microscopic characterization of scalable coherent rydberg superatoms*, Physical Review X **5**(3), 031015 (2015), doi:10.1038/nphys3835.
- [44] A. D. Bounds, N. C. Jackson, R. K. Hanley, R. Faoro, E. M. Bridge, P. Huillery and M. P. A. Jones, *Rydberg-dressed magneto-optical trap*, Phys. Rev. Lett. **120**, 183401 (2018), doi:10.1103/PhysRevLett.120.183401.
- [45] M. Khazali, H. W. Lau, A. Humeniuk and C. Simon, *Large energy superpositions via rydberg dressing*, Phys. Rev. A **94**, 023408 (2016), doi:10.1103/PhysRevA.94.023408.